The Astrophysical Journal, 771:78 (6pp), 2013 July 10 doi:10.1088/0004-637X/771/2/78

RECOMBINATION RATE COEFFICIENTS OF BORON-LIKE Ne

S. Mahmood[1], I. Orban[1], S. Ali[1], P. Glans[2], E. A. Bleda[3], Z. Altun[3], and R. Schuch[1]
[1] Department of Physics, Stockholm University, SE-10691 Stockholm, Sweden
[2] Department of Applied Sciences and Design, Mid Sweden University, SE-851 70 Sundsvall, Sweden
[3] Department of Physics, Marmara University, 81040 Istanbul, Turkey
Received 2012 October 14; accepted 2013 April 23; published 2013 June 18

ABSTRACT

Recombination of Ne^{5+} was measured in a merged-beam type experiment at the heavy-ion storage ring CRYRING. In the collision energy range 0–110 eV resonances due to $2s^22p \rightarrow 2s2p^2$ ($\Delta n = 0$) and $2s^22p \rightarrow 2s^23l$ ($\Delta n = 1$), core excitations were observed. The experimentally derived rate coefficients agree well with the calculations obtained using AUTOSTRUCTURE. At low energies, recombination is dominated by resonances belonging to the spin-forbidden $2s2p^2(^4P_J)nl$ series. The energy-dependent rate coefficients were convoluted with a Maxwell–Boltzmann electron energy distribution to obtain plasma recombination rate coefficients. The data from the literature deviate from the measured results at low temperature.

Key words: atomic data – atomic processes – plasmas

Online-only material: color figures

1. INTRODUCTION

Emission lines from the boron-like isoelectronic sequence have been observed from a wide variety of astrophysical objects, such as planetary nebulae, galaxies, interstellar medium, and the Sun (Curran 2009; Nieva & Przybilla 2008; Nataraj et al. 2007). Of particular interest is the atomic data of boron-like neon first because neon is an astrophysically abundant element (Landi & Feldman 2007; Anders & Grevesse 1989), and second experimental data for boron-like Ne do not exist so far. Neon emission lines have been used for solving the solar-model problem by observing its absolute abundances in nearby stars (Drake & Testa 2005; Cunha et al. 2006). Neon is very important for fusion plasmas, for example, high-speed neon pellets are introduced into tokamak fusion reactors to reduce the effects of plasma disruptions by intense radiation, which dumps the plasma energy very quickly on the reactor wall (Combs et al. 1996; Brooks 1996). It is also often used as a carrier gas in experiments due to its inert properties. Reliable experimental recombination data of highly charged neon are therefore essential for such applications. In particular, recombination rate coefficients of highly charged ions are important for the study and modeling of astrophysical and laboratory plasmas as well as for the interpretation of astrophysical observations.

Dielectronic recombination (DR) is considered to be an important source of emission lines from laboratory and astrophysical plasmas (Dubau & Volonté 1980; Hahn & LaGattuta 1988). This mechanism was first recognized by Burgess (1964) as being the most important and dominant recombination channel over radiative recombination (RR) in the solar corona at high temperatures. DR is a resonant process and completes in two steps. In the first step, a free electron is captured into the vacant shell of the ion, while a core electron is simultaneously excited. The produced doubly excited state decays either by autoionization or by radiative decay. The autoionization channel returns the system to the original charge state, whereas the latter process leads to the completion of DR, as a result the charge state of the ion decreases by one.

The accuracy of the derived plasma parameters from models depends crucially on the input atomic data used for the calculations. So far the majority of the DR data used in modeling is obtained by calculations and contains significant uncertainties (Kallman & Bautista 2001; Mazzotta et al. 1998; Bryans et al. 2006). For example, the recommended rate coefficients of Mazzotta et al. (1998) for B-like ions such as Ne^{5+}, Mg^{7+}, and Si^{9+} have estimated uncertainties of 70% (Savin & Laming 2002). At relatively low energies below 3 eV, the rate coefficients are very sensitive to the structure of DR resonances (Lindroth & Schuch 2003). In this energy range, the discrepancies between measured and calculated results are even larger, which lead to a profound impact on the low-temperature plasma rate coefficients. Even a small variation in low-energy DR resonance positions may induce an uncertainty of a factor 2–3 in the plasma rate coefficients (Schippers et al. 2004). The recombination rate coefficients obtained from measurements at storage rings are accurate enough and can be used to benchmark different theoretical descriptions.

The large discrepancies between experimental and calculated rate coefficient at low energy are most likely because of the simplified theoretical treatment of the many-electron problem. To calculate DR rate coefficient at lower energies, the electron correlation, as well as relativistic and quantum-electrodynamical effects, must be taken into account to high accuracy in the calculations of the involved states. These effects are very important, even for the light ions such as C IV as discussed by Mannervik et al. (1997). Second, the rate coefficients obtained by interpolation along the isoelectronic sequence of ions may also contain uncertainties because the data obtained in this way are not reliable due to a particular atomic structure of each ionic species, which differ even from the neighboring element. It is therefore necessary to evaluate the spectra of each ion on an individual basis, especially for DR at low energies.

Experimental work on electron–ion recombination has been carried out for other B-like ions, such as N^{2+}, O^{3+}, F^{4+} (Dittner et al. 1988), Ar^{13+} (DeWitt et al. 1996), Fe^{21+} (Savin et al. 2003), Mg^{7+} (Lestinsky et al. 2012), and C^{1+} (Ali et al. 2012). Electron–ion recombination of Ne ions, for example, Ne^{6+} (Orban et al. 2008), Ne^{7+} (Zong et al. 1998; Böhm et al. 2001, 2005), and Ne^{10+} (Gao et al. 1995, 1997), have been studied in storage ring experiments so far. In this paper, we report the first measurement of the recombination rate coefficient for the Ne^{5+} recombining into Ne^{4+}. The paper is organized as follows.

The experimental procedure and data analysis is outlined in Section 2. The calculation method is briefly discussed in Section 3. In Section 4, the experimental results are presented and compared with the AUTOSTRUCTURE calculations and data available in the literature. The summary and conclusions of the presented work are given in the last section of the paper.

2. EXPERIMENT AND DATA ANALYSIS

The measurement was performed at the CRYRING heavy-ion storage ring (Abrahamsson et al. 1993) at the Manne Siegbahn Laboratory in Stockholm. The Ne^{5+} ions were produced in an electron cyclotron resonance ion source and injected into the storage ring. The ions were accelerated by an RF drift tube system, to an energy of 5.89 MeV amu^{-1}. An average of 4.9×10^5 ions were stored in the ring.

In the electron cooler (Danared et al. 2000) section of the storage ring an adiabatically expanded electron beam with a diameter of 4.0 cm was merged with the ion beam over an effective distance of 0.80 m. During 2 s of electron cooling, the ion-beam phase space was reduced such that the ion beam diameter shrinks to approximately 1 mm. During electron cooling (Poth 1990), the electron-beam velocity was set equal to the average ion velocity. Hereafter, this will be referred to as cooling condition. During the measurements, the electron-beam current had a constant value of 52 mA. This corresponds to a density of 7.7×10^6 cm^{-3} at cooling condition. The electron beam temperatures were $k_B T_\parallel = 0.1$ meV and $k_B T_\perp = 1$ meV.

The electron beam in the merged-beam section also acted as a target for the circulating ions, where Ne^{5+} ions recombined with the electrons to produce Ne^{4+}. The recombined Ne^{4+} ions were separated from the stored beam in the first dipole magnet downstream the electron cooler. A surface-barrier detector with 100% efficiency was used to detect the recombined ions. For each recombined ion hitting the detector, the pulse height, the electron accelerating potential, and the cycle time were recorded. After ~4.7 s of data acquisition, the stored ions were dumped and a new ion beam injection was performed.

Following electron cooling of the ion beam, the electron beam energy was scanned in a zig-zag pattern to cover the electron–ion collision energy in the range of 0–35 eV, with electrons both faster and slower than the circulating ions. This energy range was chosen to cover the DR resonances associated with the excitation of the core electron within the same shell, i.e., $\Delta n = 0$ type DR.

After the measurement described above, the energy range was extended to cover collision energies up to 120 eV, to also include the DR resonances associated with $2s^2 2p\varepsilon l \rightarrow 2s^2 3lnl$ ($\Delta n = 1$) transitions. This spectrum was measured only in scans with electrons faster than the ions, because the beam drag force correction is not necessary here.

In order to obtain the recombination rate coefficients, the count rate $R(E)$ associated with every electron–ion collision energy was normalized to the number of ions in the ring, N_i, and the electron density, n_e,

$$\alpha(E) = \frac{R(E)\gamma^2}{N_i n_e (l_i/L_R)}, \quad (1)$$

where γ is the relativistic factor. The time fraction spent by the ions in the interaction region was accounted for by the fraction l_i/L_R, where l_i and L_R are the electron–ion interaction length and ion orbit length, respectively. The resulting spectrum was corrected for the lifetime of the ion beam and for the background signal, arising mostly from electron capture from residual gas molecules. The electron–ion collision energy in the center-of-mass system was obtained with a similar procedure as described by DeWitt et al. (1996) and Fogle et al. (2003).

The error in the rate coefficients is estimated to be less than 17% in total. It is the quadratic sum of uncertainties due to counting statistics (5%–10%), uncertainties in ion current (6%), electron–ion interaction length (8%), and estimated metastable content (9%).

3. THEORY

The resonant recombination cross sections were obtained from intermediate coupling AUTOSTRUCTURE calculations (Badnell 1986, 1987) covering the energy range associated with $\Delta n = 0$ and $\Delta n = 1$ type DR. The energies were adjusted to match spectroscopic values from the NIST atomic database (Kramida et al. 2012). The AUTOSTRUCTURE calculation contains radiative and autoionization decay rates for stabilization of the intermediate doubly excited states. The stabilization through radiative decay takes into account decay of both the excited core and the Rydberg electron. For the autoionization rates, the decay to the original state as well as all other energetically available states have been considered. Separate calculations were performed for the Rydberg electron in states with $n < 21$ and $n < 1000$. Hereafter, these two calculations will be referred to as the n_{cutoff} calculation and the field-ionization free calculation, respectively. More details about the AUTOSTRUCTURE calculations for B-like ions are given by Altun et al. (2004).

For comparison with the experimentally derived rate coefficients, the calculated cross sections $\sigma(v)$ were multiplied with the average electron velocity v_e and convoluted with the velocity distribution of the electrons in the experiment:

$$\alpha(E) = \int \sigma(v) v_e f(v_e) dv^3, \quad (2)$$

where $f(v_e)$ is the electron velocity distribution in the electron cooler with parameters given above, derived from fits to resonances.

4. RESULTS AND DISCUSSION

4.1. Merged-beam Recombination Rate Coefficients

For B-like ions, the dielectronic capture process (for $\Delta n = 0$ core excitations from the ground state) can be represented as $1s^2\ 2s^2\ 2p\ (^2P_{1/2}) + e^- \rightarrow 1s^2\ 2s\ 2p^2\ (^4P_J, {}^2D_J, {}^2S_{1/2}, {}^2P_J) n\ell$. There is thus a possibility of four $\Delta n = 0$ series in the recombination spectrum. The energy positions of the DR resonances are estimated using

$$E_e = \Delta E_{core} - Ry \frac{Q^2}{n^2}, \quad (3)$$

where E_e is the kinetic energy of the free electron, ΔE_{core} is the excitation energy of the core electron, Ry is the Rydberg constant, and Q is the ionic charge. The last term in Equation (3) gives the binding energy of the Rydberg electron in the state in which the free electron is captured (neglecting the quantum defect of different ℓ states). With the increase of kinetic energy of the free electron, for the same core excitation, the Rydberg electron will be captured into higher $n\ell$ states. The positions for

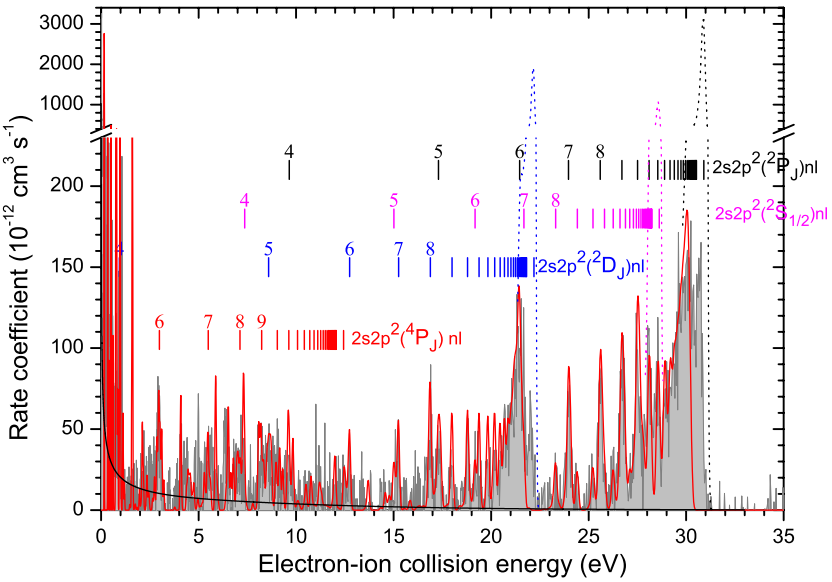

Figure 1. Comparison of experimental recombination rate coefficient of Ne VI with calculations. The experimental spectrum is shown by a gray area, while the solid and dotted lines show the results for $n_{\rm cutoff}$ and field-ionization free AUTOSTRUCTURE calculations, respectively. The vertical bars indicate approximate DR resonance energy positions calculated with Equation (3).

(A color version of this figure is available in the online journal.)

the associated DR resonances become dense as n increases, since the energy difference between consecutive n levels scales as $1/n^2$. Thus, typically, unresolved pile-up structures are formed near the series limits.

The recombination spectrum, in the energy region of 0–35 eV, corresponding to the $\Delta n = 0$ resonances in Ne^{4+}, is shown in Figure 1. Two series of peaks leading to prominent pile-up structures are observed in the spectrum. The strongest peaks belong to the $2s2p^2(^2P_J)n\ell$ series, which has its expected series limit at about 31.0 eV (Kramida et al. 2012). The $2s2p^2(^2D_J)n\ell$ series, which has its calculated series limit at 22.2 eV (Kramida et al. 2012), is also prominent in the spectrum. The $2s2p^2(^2S_{1/2})n\ell$ series, with an expected series limit at 28.6 eV (Kramida et al. 2012), is weaker. It is difficult to observe any peaks from this series in the spectrum because these are weak and overlap with the other two series. However, the AUTOSTRUCTURE calculation suggests that some small peaks from the $2s2p^2(^2S_{1/2})n\ell$ series are observed in the experimental spectrum in Figure 1 at energies between 23 and 27 eV.

A pile-up structure is not observed for the "spin-forbidden" $2s2p^2(^4P_J)n\ell$ series. Both the autoionization rates and the radiative rates for the resonances belonging to this series decreases rapidly with increasing n and the contribution from high-n states is negligible, and, hence, no pile-up structure is observed near the series limit at about 12.5 eV (Kramida et al. 2012). However, for low-n states ($6 \leqslant n \leqslant 11$) the radiative rates and autoionization rates are high enough to yield some fairly intense resonances. Thus, below 10 eV, peaks due to this series are prominent. In fact, a large portion of the intensity below 10 eV is due to $2s2p^2(^4P_J)n\ell$ resonances.

DR resonances associated with the excitation of a core electron from the ground state ($^2P_{1/2}$) to the first excited state ($^2P_{3/2}$) are not observed. The energy difference between these states is 162.02 meV. The energy balance requires for the electron to be captured into states with $n \geqslant 46$, according to Equation (3). Due to field ionization of $n \geqslant 21$, the ions return to their original charge states and these resonances are therefore not detected. Moreover, calculations show that the intensity of these resonances is very weak and they cannot contribute significantly to the spectrum.

For comparison of the experimentally derived results with calculations, the RR contribution to the measured rate coefficient was estimated. The RR cross section can be calculated by Kramers formula (Kramers 1923)

$$\sigma_n(E) = 2.105 \times 10^{-22}\, g_n \frac{Ry^2 Z_{\rm eff}^4}{nE\left(n^2E + RyZ_{\rm eff}^2\right)}\ {\rm cm}^2, \qquad (4)$$

where $Z_{\rm eff}$ is the effective charge of the ion, E is the center-of-mass energy, n is the principal quantum number of the recombined electron, and g_n is the Gaunt factor (Seaton 1959) to account for a discrepancy between classical and quantum-mechanical descriptions at lower n states. For Ne^{5+} ions a value of $Z_{\rm eff}$ of 7.5 was used (McLaughlin & Hahn 1991). The total RR cross section was obtained by summation over all available n states. The RR rate coefficient as a function of energy is obtained by convoluting the cross sections using Equation (2), and it is shown by the blue dashed line in Figure 2(a). It agrees quite well in absolute height and slope with the measured background rate.

The calculated DR rate coefficients using AUTOSTRUCTURE are shown in Figure 1 by solid and dotted lines for the $n_{\rm cutoff}$ calculation and the field-ionization free calculation, respectively. Recombined ions with the outer electron in a Rydberg orbital with $n > n_{\rm cutoff} = 21$ are field ionized due to the motional electric field in the dipole magnet and they are, therefore, not detected. In the experiment, the flight time between the electron cooler and the first dipole magnet was about 60 ns. An ion which recombines via a state with $n > n_{\rm cutoff}$ will only be detected in the experiment if, through radiative decay, it reaches a state with the outer electron in $n \leqslant n_{\rm cutoff}$ during this flight time. The $n_{\rm cutoff}$ calculation corresponds to a case where all recombined ions with $n > n_{\rm cutoff}$ are field ionized, and the field-ionization free calculation corresponds to the case of no field ionization (i.e., the case of no external fields). By comparing the experimental spectrum with the two calculated spectra, for example, at 30–31 eV in Figure 1, it is apparent

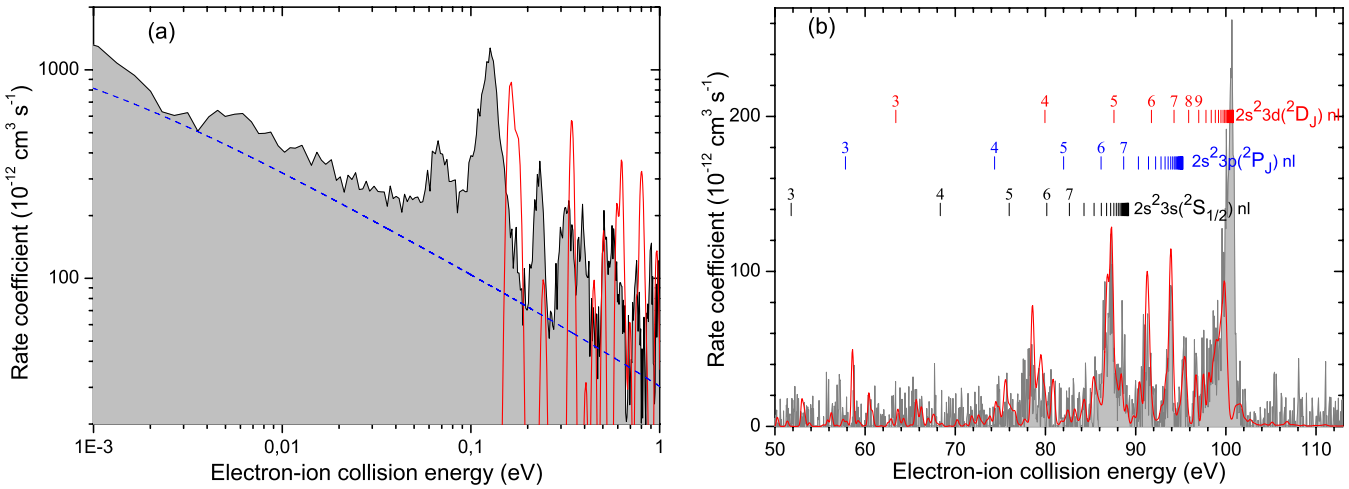

Figure 2. (a) Recombination rate coefficient of Ne VI at low energy. The gray area shows the experimental results. The red line denotes the calculations using AUTOSTRUCTURE. The blue dashed line represents the calculated RR contribution. (b) Recombination rate coefficient of Ne VI in the energy region corresponding to $\Delta n = 1$ core excitation. The vertical bars indicate estimated DR resonance energy positions, calculated with Equation (3).

(A color version of this figure is available in the online journal.)

that there is some contribution from states with $n > n_{\rm cutoff}$ in the experimental spectrum (because of radiative decay involving the outer electron during the 60 ns flight time) although the contribution is much smaller than what one would expect in the field-ionization-free case.

The experimentally derived rate coefficient agrees rather well with the AUTOSTRUCTURE calculations in the energy range 4–23 eV (see Figure 1). In deriving the absolute recombination rate coefficients, the contamination by metastable ions in the stored ion beam is an issue of concern. For Ne^{5+} ions, the lifetimes of metastable states $2s2p^2$ ($^4P_{1/2,\ 3/2,\ 5/2}$) are in the range of 38–307 μs (Rynkun et al. 2012). These states will not survive during the cooling phase of the beam, which lasts for 2 s. Therefore, these excited states are not expected to contribute when the electron energy scan starts. However, the lifetime of the lowest excited state $2s^2 2p$ ($^2P_{3/2}$) is 49 s (Rynkun et al. 2012). Ions produced in the source in this metastable state can survive transport, acceleration, and cooling in the storage ring. Thus there exists a fraction of the primary Ne^{5+} ion beam in this metastable state during the measurements.

Separate calculations were performed for ions initially in the ground state and in the $2s^2 2p\ ^2P_{3/2}$ metastable state. In order to correct for the metastable fraction, the ground-state AUTOSTRUCTURE calculations were scaled to match the experimentally derived results in the energy range from 23 to 31 eV. The scaling factor is 0.83, which suggests that 17% ions are in the metastable state. This estimated metastable fraction is supported by other experiments at CRYRING, such as 14% $^3P_0$ metastable fraction of Ne^{6+} ions (Orban et al. 2008) and 15% $^2P_{3/2}$ fraction of F^{5+} ions (Ali et al. 2012).

In Figure 2(a), the rate coefficients at low energy <1 eV are shown. The gray area and red line depict the experimental and calculated rate coefficients, respectively. The calculated intensities and energy positions of the resonances, in this low-energy region, agree poorly with the measurements. This disagreement is probably due to electron correlation that is not fully accounted for in the calculations.

The $\Delta n = 1$ type DR resonances are associated with the excitation of a $2p$ electron to one of the 3ℓ orbitals. The corresponding experimentally derived rate coefficients for Ne^{5+} are shown in Figure 2(b) in the energy range 50–112 eV. The red lines denote the calculated spectrum and the vertical bars indicate estimated DR resonance energy positions, calculated using Equation (3). The calculated rate coefficients agree well with the experimental values except near the series limit at 101.2 eV (Kramida et al. 2012) of the $2s^2 3d(^2D_J)n\ell$ series. According to our AUTOSTRUCTURE calculations the contribution from high-n states, with $n > n_{\rm cutoff}$, is negligible, and therefore the $n_{\rm cutoff}$ calculation and the field-ionization free calculation basically yield identical results. However, our experimental spectrum show a strong peak at about 100 eV, in the energy region where you would expect contribution from high-n states belonging to the $2s^2 3d(^2D_J)n\ell$ series. The strong peak at about 100 eV peak is not reproduced by the calculations, as can be seen in Figure 2(b).

4.2. Plasma Recombination Rate Coefficients

In order to obtain plasma recombination rate coefficients, $\alpha(T_e)$, the merged-beam rate coefficients were convoluted with a Maxwell–Boltzmann energy distribution (Savin 1999)

$$\alpha(T_e) = \int \alpha(E) f(E, T_e) dE \qquad (5)$$

where $\alpha(E)$ is the merged-beam recombination rate coefficient, and $f(E, T_e)$ is the electron Maxwell–Boltzmann energy distribution for a given plasma temperature T_e

$$f(E, T_e) = \frac{2E^{1/2}}{\pi^{1/2}(k_B T_e)^{1/2}} \exp\left(-\frac{E}{k_B T_e}\right), \qquad (6)$$

where k_B is the Boltzmann constant. This folding is valid if the velocity spread of the electron beam is much smaller than the width of the electron energy distribution in the plasma (Schippers et al. 2001).

In order to obtain the DR plasma rate coefficients, the contribution of RR, shown by the dotted line in Figure 2(a), was subtracted from the experimentally derived spectrum. The resulting spectrum up to the $2s^2 3d(^2D_J)nl$ series limit is then convoluted using Equation (5). The derived DR plasma rate coefficients are shown in Figure 3 by the solid line.

The experimentally derived recombination rate coefficients are affected by the field-ionization of high-n states, as discussed in the previous section. Field-ionization-free plasma rate

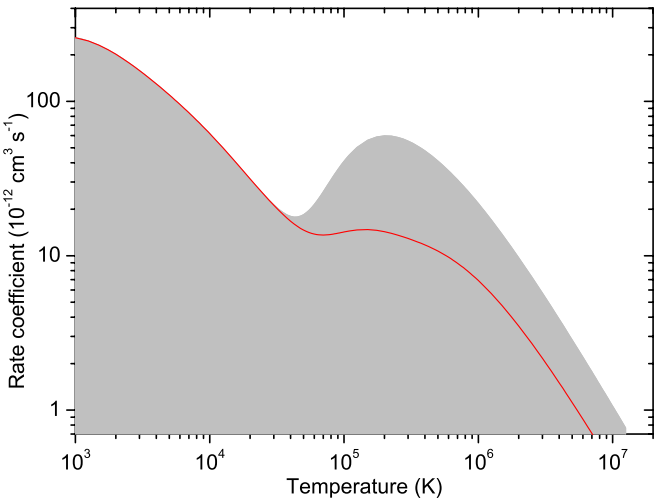

Figure 3. DR plasma rate coefficients for Ne VI are shown as a function of temperature. The solid (red) line shows the plasma rate coefficients derived directly from the experimental spectrum. Note that the contribution from the high-n states is reduced in the experimental spectrum due to field ionization. The gray area shows the field-ionization free plasma rate coefficients, obtained using the rate coefficients from the experimental spectrum and correcting the coefficients in the energy regions of high-n states using scaled rate coefficients from the field-ionization free calculation.

(A color version of this figure is available in the online journal.)

coefficients were derived by using a similar procedure as described by Schippers et al. (2001), and Fogle et al. (2005). The contributions from the high-n states ($n > n_{\rm cutoff}$) were estimated using the rate coefficients from the field-ionization free calculation. The resulting energy-dependent spectrum is obtained by replacing the field affected parts in the experimental rate-coefficient spectrum with the scaled rate coefficients from the calculation. The field-ionization-free plasma rate coefficients were derived by convoluting the resulting spectrum using Equation (5) and the obtained coefficients are shown in Figure 3 by the gray area.

At low temperature, $T < 3\times10^4$ K, the two curves are identical since recombination into low Rydberg states dominates. For higher temperatures, $T > 3 \times 10^4$ K, the contribution from high-n states is significant and the field-ionization-free plasma rate coefficients are much higher than the coefficients obtained directly from the (field-ionization affected) experimental spectrum.

For use in plasma applications the field-ionization-free rate coefficients were fitted with the following expression for DR rate coefficients originally suggested by Burgess (1965),

$$\alpha(T_e) = T_e^{-\frac{3}{2}} \sum_i c_i \exp\left(-\frac{E_i}{k_B T_e}\right) \qquad (7)$$

where the coefficients c_i and E_i are fit parameters. The obtained fit parameters are given in Table 1.

The experimentally derived field-ionization-free plasma rate coefficients are shown in Figure 4 along with data available in the literature. The DR rate coefficients are represented by the solid line and the total (RR+DR) rate coefficients by the gray area. Below a temperature of 8×10^4 K the RR contribution is significant. Temperature intervals for photoionized and collisionally ionized plasma, where the concentration of Ne^{5+} is higher than 10% of the maximum abundance, are shown by the vertical dashed lines (Kallman & Bautista 2001).

The calculated values of Nahar (1995), as shown by circles, contain contributions from both RR and DR (unified approach) and they are in good agreement with our field-ionization-free values (gray area) in the temperature range 10^3–5×10^5 K. Above 10^6 K Nahar values are significantly higher than our values.

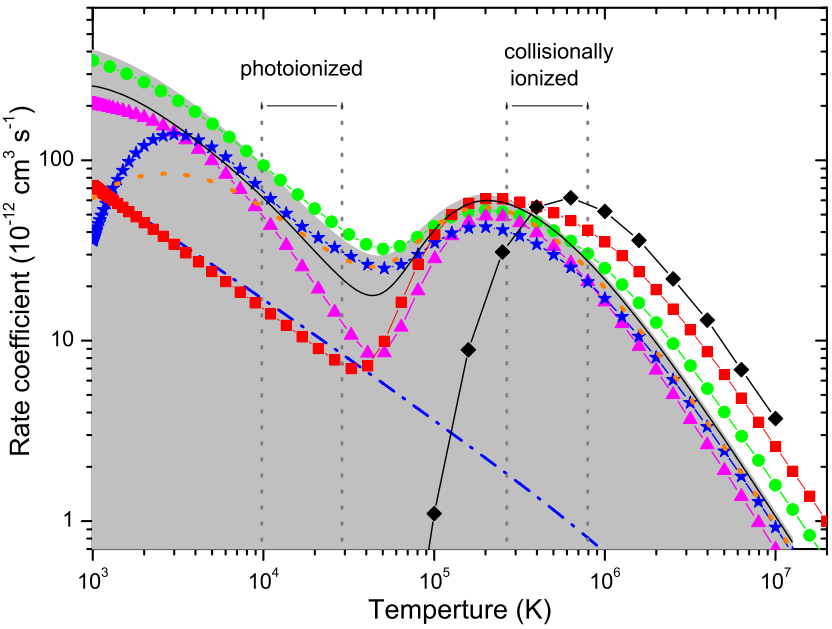

Figure 4. Plasma rate coefficient for Ne VI as a function of temperature. The vertical dashed lines indicate the temperature intervals for the photoionized and collisionally ionized plasma regions (Kallman & Bautista 2001). The gray area and black solid line represent our field-ionization free total (RR+DR) and DR rate coefficients, respectively. The orange dotted line shows the results from our field-ionization free AUTOSTRUCTURE calculation. The calculated plasma rate coefficients from the literature are denoted as follows: stars, Altun et al. (2004); circles, Nahar (1995); squares, Shull & Steenberg (1982); triangles, Mazzotta et al. (1998); and diamond, Jacobs et al. (1979). The results from Nahar include contribution from both RR and DR. The RR plasma rate coefficients from Badnell (2006) are shown by the blue dash-dotted line.

(A color version of this figure is available in the online journal.)

Table 1
Fit Parameters for DR Plasma Rate Coefficients

No.	Field Effected DR Data		Field-ionization-free DR Data	
i	c_i	E_i	c_i	E_i
1	2.5848 [−4]	8.3783	6.0657 [−5]	1.2303
2	2.1828 [−5]	2.5028	8.7152 [−5]	5.4109
3	3.4700 [−5]	0.3887	6.8779 [−3]	27.908
4	2.6403 [−5]	0.1053	1.0542 [−2]	89.496
5	5.6331 [−5]	1.1308	3.5581 [−5]	0.4072
6	1.0487 [−2]	92.069	2.6365 [−5]	0.1066
7	3.5126 [−3]	25.068	1.3735 [−3]	15.343
8	3.8572 [−4]	20.426	1.0437 [−2]	28.306
9			5.0784 [−3]	27.375

Notes. The units of c_i and E_i are $cm^3\ s^{-1}\ K^{3/2}$ and eV, respectively. Numbers in square brackets denote the powers of 10. The fit parameters for the field effected and field-ionization free DR data are obtained from the solid curve and gray area curve in Figure 3, respectively.

At a temperature of 5×10^5 K the rate coefficients from Nahar are 35% higher than experimentally derived rate coefficients.

The DR plasma rate coefficients of Mazzotta et al. (1998), as shown by triangles, deviate from the experimentally derived DR rate coefficients (solid line) for the investigated temperature range. Particularly the calculations of Mazzotta et al. (1998) significantly underestimate the plasma rate coefficients in the temperature range 1.5×10^4–10^5 K. Above a temperature of 2×10^5 K, the experimental values are 40% larger than results of Mazzotta et al. (1998).

The DR plasma rate coefficients from Altun et al. (2004), as shown by stars, are in good agreement with our results for temperatures greater than 10^6 K. However, their calculations overestimate the rate coefficients at about 2×10^4 to 6×10^4 K and underestimate the rate coefficients in the temperature range 10^5–10^6 K. Particularly, the calculations severely underestimate the rate coefficients at low temperatures, below 3×10^3 K. The discrepancy at low temperatures is probably due to an underestimation of DR resonances at very low energies <1 eV in the calculations by Altun et al. (2004), as shown and discussed also with Figure 2(a).

The data of Shull & Steenberg (1982), as shown by squares, include rate coefficients only due to RR for $T < 3\times10^4$ K and DR for $T > 3\times10^4$ K. Their predictions are in poor agreement with our results for $T > 4\times10^5$ K. Jacobs et al. (1979) reported results, as shown by diamonds, only for higher temperatures. The calculated values by Jacobs et al. are in poor agreement with our experimentally derived results and with the results of the other calculations, as shown in Figure 4.

5. CONCLUSIONS

Recombination rate coefficients of B-like Ne recombining into C-like Ne were obtained for the first time in a measurement performed at the CRYRING heavy-ion storage ring. Good agreement was found between experimentally derived rate coefficients and results of AUTOSTRUCTURE calculations in the energy range of 4–23 eV dominated by the $\Delta n = 0$ type DR resonances. At low energy <1 eV the results disagree both in the energy positions and the intensities of the resonances. Resonances for $\Delta n = 1$ transitions were observed between 50 and 110 eV. The calculations severely underestimate the intensity in the energy range of 98–101 eV. The experimentally derived plasma rate coefficients show the same trend as predicted by some of the calculations.

We acknowledge financial support from the Knut and Alice Wallenberg Foundation and the Swedish Research Council VR. We are grateful to the CRYRING crew for their excellent support during the experiment.

REFERENCES

Abrahamsson, K., Andler, G., Bagge, L., et al. 1993, NIMPB, 79, 269
Ali, S., Orban, I., Mahmood, S., et al. 2012, ApJ, 753, 132
Ali, S., Orban, I., Mahmood, S., Loch, S. D., & Schuch, R. 2012, A&A, submitted
Altun, Z., Yumak, A., Badnell, N. R., Colgan, J., & Pindzola, M. S. 2004, A&A, 420, 775
Anders, E., & Grevesse, N. 1989, GeCoA, 53, 197
Badnell, N. R. 1986, JPhB, 19, 3827
Badnell, N. R. 1987, JPhB, 20, 2081
Badnell, N. R. 2006, ApJ, 167, 334
Böhm, S., Müller, A., Schippers, S., et al. 2005, A&A, 437, 1151
Böhm, S., Schippers, S., Shi, W., et al. 2001, PhRvA, 64, 032707
Brooks, J. N. 1996, PhPl, 3, 2286
Bryans, P., Badnell, N. R., Gorczyca, T. W., et al. 2006, ApJS, 167, 343
Burgess, A. 1964, ApJ, 139, 776
Burgess, A. 1965, ApJ, 141, 1588
Combs, S. K., Love, T. L., Jernigan, T. C., et al. 1996, RScI, 67, 837
Cunha, K., Hubeny, I., & Lanz, T. 2006, ApJL, 647, L143
Curran, S. J. 2009, A&A, 497, 351
Danared, H., Källberg, A., Andler, G., et al. 2000, NIMPA, 441, 123
DeWitt, D. R., Schuch, R., Gao, H., et al. 1996, PhRvA, 53, 2327
Dittner, P. F., Datz, S., Hippler, R., Krause, H. F., & Miller, P. D. 1988, PhRvA, 38, 2762
Drake, J. J., & Testa, P. 2005, Natur, 436, 525
Dubau, J., & Volonté, S. 1980, RPPh, 43, 199
Fogle, M., Badnell, N. R., Glans, P., et al. 2005, A&A, 442, 757
Fogle, M., Eklöw, N., Lindroth, E., et al. 2003, JPhB, 36, 2563
Gao, H., DeWitt, D. R., Schuch, R., et al. 1995, PhRvL, 75, 4381
Gao, H., Schuch, R., Zong, W., et al. 1997, JPhB, 30, L499
Hahn, Y., & LaGattuta, K. J. 1988, PhR, 166, 195
Jacobs, V. L., Davis, J., Rogerson, J. E., & Blaha, M. 1979, ApJ, 230, 627
Kallman, T., & Bautista, M. 2001, ApJS, 133, 221
Kramers, H. A. 1923, PMag, 46, 836
Kramida, A., Ralchenko, Yu., Reader, J., & NIST ASD Team., 2012, NIST Atomic Spectra Database (ver. 5.0), http://physics.nist.gov/asd
Landi, E., & Feldman, U. 2007, ApJ, 659, 743
Lestinsky, M., Badnell, N. R., Bernhardt, D., et al. 2012, ApJ, 758, 40
Lindroth, E., & Schuch, R. 2003, The Physics of Multiply and Highly Charged Ions, Vol. 1 (Netherlands: Kluwer), 231
Mazzotta, P., Mazzitelli, G., Colafrancesco, S., & Vittorio, N. 1998, A&A, 133, 403
McLaughlin, D. J., & Hahn, Y. 1991, PhRvA, 43, 1313
Mannervik, S., Asp, S., Broström, L., et al. 1997, PhRvA, 55, 1810
Nahar, S. N. 1995, ApJS, 101, 423
Nataraj, H. S., Sahoo, B. K., Das, B. P., Chaudhuri, R. K., & Mukherjee, D. 2007, JPhB, 40, 3153
Nieva, M. F., & Przybilla, N. 2008, A&A, 481, 199
Orban, I., Böhm, S., Loch, S. D., & Schuch, R. 2008, A&A, 489, 829
Poth, H. 1990, PhR, 196, 135
Rynkun, P., Jönsson, P., Gaigalas, G., & Froese Fischer, C. 2012, ADNDT, 98, 481
Savin, D. W. 1999, ApJ, 523, 855
Savin, D. W., & Laming, J. M. 2002, ApJ, 566, 1166
Savin, D. W., Kahn, S. M., Gwinner, G., et al. 2003, ApJS, 147, 421
Schippers, S., Müller, A., Gwinner, G., et al. 2001, ApJ, 555, 1027
Schippers, S., Schnell, M., Brandau, C., et al. 2004, A&A, 421, 1185
Seaton, M. J. 1959, MNRAS, 119, 81
Shull, J. M., & Steenberg, M. V. 1982, ApJS, 48, 95
Zong, W., Schuch, R., Gao, H., DeWitt, D. R., & Badnell, N. R. 1998, JPhB, 31, 3729